POLITECNICO
DI MILANO

RE.PUBLIC@POLIMI

Research Publications at Politecnico di Milano

Post-Print

This is the accepted version of:

The final publication is available at http://dx.doi.org/10.2514/1.G001080

Access to the published version may require subscription.

When citing this work, cite the original published paper.

Low-Thrust Minimum Fuel Optimization in the Circular Restricted Three-Body Problem

Chen Zhang[1]
Beihang University, Beijing, People's Republic of China, 100191

Francesco Topputo[2] and Franco Bernelli-Zazzera[3]
Politecnico di Milano, Milano, Italy, 20156

Yu-Shan Zhao[4]
Beihang University, Beijing, People's Republic of China, 100191

I. Introduction

The challenging missions envisioned for the upcoming decades involve innovative spacecraft trajectory concepts. For instance, installing outposts at Earth–Moon Lagrange points requires novel transfers. These orbits shall, at minimum, be able to combine the benefits inherent to multi-body dynamics with those enabled by advanced propulsion technologies. The three-body dynamics already suffice to produce free transport mechanisms, whereas the high specific impulse typical of low-thrust propulsion allows considerable propellant savings. The challenge is then to design optimal low-thrust, three-body transfers.

This subject has recently gained the attention of the scientific community. In [1] design synthesis is achieved by combining invariant manifolds and attainable sets, which are sets containing ballistic and low-thrust orbits, respectively. In [2] transfers to distant periodic orbits have been designed by targeting their invariant manifolds with low-thrust propulsion. Using invariant manifolds as a first guess solution in high-fidelity, low-thrust optimization was examined in [3]. Low-energy, low-thrust

---

[1] Ph.D. Candidate, School of Astronautics; `buaa_zc@sa.buaa.edu.cn`.
[2] Assistant Professor, Department of Aerospace Science and Technolgy; `francesco.topputo@polimi.it`.
[3] Professor, Department of Aerospace Science and Technolgy; `franco.bernelli@polimi.it`.
[4] Professor, School of Astronautics; `yszhao@buaa.edu.cn`.

transfers to the Moon have been formulated in [4, 5]. Low-thrust optimization in a three-body model was studied also in [6–10] without relying on invariant manifolds. These concepts were demonstrated by SMART-1 [11], where the pioneering ideas in [12] were applied.

In this field, the case of low-thrust transfers to Earth–Moon Lagrange point orbits is of interest. As the latter are chosen as ideal target for a number of future applications [13–15], it is crucial to assess their accessibility in terms of cost and time. In doing so, it is worth considering departure from a geostationary transfer orbit (GTO). This orbit is chosen because launch vehicles are optimized for GTO, and the case of piggy back spacecraft may also be accounted for. Nevertheless, finding an optimal low-thrust trajectory from GTO to Lagrange point orbits in the Earth–Moon system is particularly challenging because of: 1) the long-duration nature of the solutions, 2) the high number of revolutions, 3) the strong nonlinearities in the three-body vector field, 4) the high number of bang-bang structures in the optimal guidance law. These features have prevented finding end-to-end optimal transfers, and some sort of approximations, leading to suboptimal solutions, have been favored over optimality. In [16], the transfer orbit is defined by patching together a tangential thrust spiral with a leg targeting a portion of the stable manifold associated to the final orbit. As optimization is carried out in the second phase only, overall optimality is lost. The same idea is replicated in a number of later works [17–20]. Alternatively, much higher initial orbits are chosen [10, 21–24], yet not matching practical applications.

In this Note, the complete optimal low-thrust GTO-to-Halo transfer is solved for the first time. This result is achieved with an indirect approach and constant specific impulse engine. Thrust-to-mass ratios in agreement with currently available technology are considered. Some effective techniques are applied to cope with problem complexity. These methods involve solving the minimum-fuel, minimum-energy, and minimum-time problems [10, 25], implementing energy-to-fuel homotopy [10, 26–28], continuing the maximum thrust magnitude [10], computing the analytic Jacobians [9], and accurately detecting the switching points through a combination of Newton and bisection methods [29]. In the present approach the solution structure is not prescribed (as in [16–18, 20, 30, 31]), but rather it is found a posteriori, with low-thrust propulsion which is free to act everywhere; the final coast arc, recalling a stable manifold branch, is found automatically. The techniques presented

in this Note are useful in practical cases where very low-thrust accelerations are used for long times in highly nonlinear vector fields.

The Note is organized as follows. In Section II, the dynamical model is presented, and the minimum-fuel, minimum-energy, and minimum-time problems are stated. In Section III, the analytical Jacobians for the minimum-energy and minimum-fuel problems are derived. In Section IV, the original, hybrid switching detection technique is presented, and details on practical implementation are given. The case study is solved in Section V and critical analysis is conducted.

II. Statement of the Problem

A. Controlled Restricted Three-Body Problem

The circular restricted three-body problem studies the motion of a massless spacecraft, P_3, under the gravitational field generated by two primaries P_1, P_2 of masses m_1, m_2, respectively, which move in circular motion due to their mutual interaction. The dynamics are written in a rotating frame with non-dimensional units: the angular velocity of P_1, P_2, their distance, and the sum of their masses are all set to unity. The Earth–Moon model is considered in this work, where $\mu = m_2/(m_1 + m_2) \simeq 0.012$. The Earth, of mass $(1 - \mu)$, is located at $(-\mu, 0, 0)$, whereas the Moon, of mass μ, is located at $(1 - \mu, 0, 0)$; see [32] for details. When low-thrust propulsion is considered, it is convenient to write the equations of motions as [9]

$$\dot{\boldsymbol{x}} = \boldsymbol{f}(\boldsymbol{x}, \boldsymbol{\alpha}, u) \quad \Rightarrow \quad \begin{bmatrix} \dot{\boldsymbol{r}} \\ \dot{\boldsymbol{v}} \\ \dot{m} \end{bmatrix} = \begin{bmatrix} \boldsymbol{v} \\ \boldsymbol{g}(\boldsymbol{r}) + \boldsymbol{h}(\boldsymbol{v}) + u\,T_{\max}\,\boldsymbol{\alpha}/m \\ -u\,T_{\max}/c \end{bmatrix}, \tag{1}$$

where $\boldsymbol{r} = [x, y, z]^\top$ and $\boldsymbol{v} = [v_x, v_y, v_z]^\top$ are the spacecraft position and velocity vectors, respectively, m denotes the spacecraft mass, $T_{\max}$ is the maximum thrust magnitude, $c = I_{\mathrm{sp}}\,g_0$ represents the exhaust velocity (I_{sp} is the thruster specific impulse and g_0 is the gravitational acceleration at the sea level). The control variables are the throttle factor, $u \in [0, 1]$, and the thrust direction unit

vector, $\boldsymbol{\alpha}$. The functions $\boldsymbol{g}(\boldsymbol{r})$ and $\boldsymbol{h}(\boldsymbol{v})$ are defined as [1, 18]

$$\boldsymbol{g}(\boldsymbol{r}) = \begin{bmatrix} x - (1-\mu)(x+\mu)/r_1^3 - \mu(x+\mu-1)/r_2^3 \\ y - (1-\mu)y/r_1^3 - \mu y/r_2^3 \\ -(1-\mu)z/r_1^3 - \mu z/r_2^3 \end{bmatrix}, \quad \boldsymbol{h}(\boldsymbol{v}) = \begin{bmatrix} 2v_y \\ -2v_x \\ 0 \end{bmatrix}, \tag{2}$$

where r_1 and r_2 represent the distance of P_3 to the Earth and Moon, respectively; i.e.,

$$r_1 = \left[(x+\mu)^2 + y^2 + z^2\right]^{1/2}, \quad r_2 = \left[(x+\mu-1)^2 + y^2 + z^2\right]^{1/2}. \tag{3}$$

B. Construction of the Shooting Function

In minimum-fuel problems, a solution of (1) minimizes

$$J_f = \frac{T_{\max}}{c} \int_{t_i}^{t_f} u \ \mathrm{d}t, \tag{4}$$

where t_i, t_f denote the initial, final time, respectively. In these problems u is either zero or one [33]. This dichotomy causes discontinuities in the shooting function [28], and poses severe restrictions on numerical methods. A smoothing technique, or homotopic approach, was introduced in [26] to relax the control profile and to enforce discontinuity in a gradual way [34]. It consists in using the objective function

$$J = \frac{T_{\max}}{c} \int_{t_i}^{t_f} \left[u - \varepsilon u(1-u)\right] \ \mathrm{d}t, \quad \varepsilon \in [0, 1]. \tag{5}$$

The minimum-energy problem ($\varepsilon = 1$) is solved first; the solution is then continued by decreasing ε until (4) is reached ($\varepsilon = 0$) [28]. In this work, optimal transfers between two given states (a point on the GTO, $(\boldsymbol{r}_i, \boldsymbol{v}_i)$, and a point on the L_1 halo, $(\boldsymbol{r}_f, \boldsymbol{v}_f)$) are designed, and therefore the boundary conditions read

$$\begin{aligned} \boldsymbol{r}(t_i) - \boldsymbol{r}_i = 0, \quad \boldsymbol{v}(t_i) - \boldsymbol{v}_i = 0, \quad m(t_i) - 1 = 0, \\ \boldsymbol{r}(t_f) - \boldsymbol{r}_f = 0, \quad \boldsymbol{v}(t_f) - \boldsymbol{v}_f = 0, \end{aligned} \tag{6}$$

where the initial mass is scaled to one, whereas the final mass is obviously unconstrained. The fixed terminal state formulation in (6), as opposed to that in [16, 18, 22–24], has been chosen to favor convergence. To vary the arrival point on the Halo orbit, an outer loop can be implemented, or a problem accounting for free terminal conditions can be stated.

The Hamiltonian of the problem is [35]

$$H = \boldsymbol{\lambda}_r \cdot \boldsymbol{v} + \boldsymbol{\lambda}_v \cdot \left[\boldsymbol{g}(\boldsymbol{r}) + \boldsymbol{h}(\boldsymbol{v}) + \frac{u\,T_{\max}}{m}\boldsymbol{\alpha} \right] - \lambda_m \frac{u\,T_{\max}}{c} + \frac{T_{\max}}{c} \left[u - \varepsilon u(1-u) \right], \qquad (7)$$

where $\boldsymbol{\lambda} = [\boldsymbol{\lambda}_r, \boldsymbol{\lambda}_v, \lambda_m]^\top$ is the vector of costates, whose dynamics are

$$\dot{\boldsymbol{\lambda}} = -\frac{\partial H}{\partial \boldsymbol{x}} \quad \Rightarrow \quad \begin{bmatrix} \dot{\boldsymbol{\lambda}}_r \\[2mm] \dot{\boldsymbol{\lambda}}_v \\[2mm] \dot{\lambda}_m \end{bmatrix} = \begin{bmatrix} -\boldsymbol{G}^\top \boldsymbol{\lambda}_v \\[2mm] -\boldsymbol{\lambda}_r - \boldsymbol{H}^\top \boldsymbol{\lambda}_v \\[2mm] u\,T_{\max}/m^2 \boldsymbol{\lambda}_v \cdot \boldsymbol{\alpha} \end{bmatrix}, \qquad (8)$$

with $\boldsymbol{G} = \partial \boldsymbol{g}(\boldsymbol{r})/\partial \boldsymbol{r}$ and $\boldsymbol{H} = \partial \boldsymbol{h}(\boldsymbol{v})/\partial \boldsymbol{v}$ (only nonzero elements listed),

$$G_{1,1} = 1 - (1-\mu)/r_1^3 + 3(1-\mu)(x+\mu)^2/r_1^5 - \mu/r_2^3 + 3\mu(x+\mu-1)^2/r_2^5,$$

$$G_{2,2} = 1 - (1-\mu)/r_1^3 + 3(1-\mu)y^2/r_1^5 - \mu/r_2^3 + 3\mu y^2/r_2^5,$$

$$G_{3,3} = -(1-\mu)/r_1^3 + 3(1-\mu)z^2/r_1^5 - \mu/r_2^3 + 3\mu z^2/r_2^5,$$

$$G_{1,2} = G_{2,1} = 3(1-\mu)(x+\mu)y/r_1^5 + 3\mu(x+\mu-1)y/r_2^5,$$

$$G_{1,3} = G_{3,1} = 3(1-\mu)(x+\mu)z/r_1^5 + 3\mu(x+\mu-1)z/r_2^5,$$

$$G_{2,3} = G_{3,2} = 3(1-\mu)yz/r_1^5 + 3\mu yz/r_2^5, \quad H_{1,2} = -H_{2,1} = 2.$$

Due to (6), the boundary conditions for the costates are all unknown except for λ_m. As the final mass is free, its associated costate must be zero at t_f [35], i.e.,

$$\lambda_m(t_f) = 0. \qquad (9)$$

Conditions on the control variables u, $\boldsymbol{\alpha}$ are derived by applying the Pontryagin Maximum Principle (PMP) [36], which states that the Hamiltonian is minimized along an optimal trajectory. Since $u\,T_{\max}/m \geq 0$ in (7), then the optimal thrust direction is [37]

$$\boldsymbol{\alpha}^* = -\boldsymbol{\lambda}_v/\lambda_v. \qquad (10)$$

Substituting Eq. (10) into Eq. (7) yields

$$H = \boldsymbol{\lambda}_r \cdot \boldsymbol{v} + \boldsymbol{\lambda}_v \cdot \left[\boldsymbol{g}(\boldsymbol{r}) + \boldsymbol{h}(\boldsymbol{v}) \right] + \frac{u\,T_{\max}}{c} \left(S - \varepsilon + \varepsilon u \right), \qquad (11)$$

where a switching function, S, is defined as

$$S = -\lambda_v \frac{c}{m} - \lambda_m + 1, \qquad (12)$$

along with its first derivative

$$\dot{S} = \frac{c}{m} \frac{(-\boldsymbol{\lambda}_r - \boldsymbol{H}^\top \boldsymbol{\lambda}_v) \cdot \boldsymbol{\lambda}_v}{\lambda_v}. \tag{13}$$

The throttle factor u is the only decision variable in Eq. (11). Its value can be related to $\boldsymbol{x}$, $\boldsymbol{\lambda}$ by applying again the PMP. The optimal value, u^*, can be stated in terms of S through

$$
\begin{aligned}
u^* &= 0 && \text{if } S > \varepsilon \\
u^* &= (\varepsilon - S)/2\varepsilon && \text{if } -\varepsilon \leq S \leq \varepsilon \\
u^* &= 1 && \text{if } S < -\varepsilon.
\end{aligned}
\tag{14}
$$

Note that in minimum-fuel problems ($\varepsilon = 0$) the magnitude of u^* depends only upon the sign of S, and a bang-bang profile is generated.

Once the optimal control variables $\boldsymbol{\alpha}^*$, u^* are determined as functions of the states and costates, through Eqs. (10) and (14), the motion can be integrated implicitly with dynamics

$$\dot{\boldsymbol{y}} = \boldsymbol{F}(\boldsymbol{y}) \quad \Rightarrow \quad
\begin{bmatrix} \dot{\boldsymbol{r}} \\ \dot{\boldsymbol{v}} \\ \dot{m} \\ \dot{\boldsymbol{\lambda}}_r \\ \dot{\boldsymbol{\lambda}}_v \\ \dot{\lambda}_m \end{bmatrix}
=
\begin{bmatrix} \boldsymbol{v} \\ \boldsymbol{g}(\boldsymbol{r}) + \boldsymbol{h}(\boldsymbol{v}) - (\boldsymbol{\lambda}_v/\lambda_v)u\,T_{\max}/m \\ -u\,T_{\max}/c \\ -\boldsymbol{G}^\top \boldsymbol{\lambda}_v \\ -\boldsymbol{\lambda}_r - \boldsymbol{H}^\top \boldsymbol{\lambda}_v \\ -\lambda_v u\,T_{\max}/m^2 \end{bmatrix}. \tag{15}$$

where $\boldsymbol{y} = [\boldsymbol{x}, \boldsymbol{\lambda}]^\top$ is a 14-dimensional canonical variable [9]. A two-point boundary value problem (TPBVP) is defined by (15) together with the boundary conditions (6) and (9). If the initial costate vector $\boldsymbol{\lambda}_i$ was given, one could integrate (15) (with u as in (14)) and check if the final conditions are verified. In the likely case in which these are not met, $\boldsymbol{\lambda}_i$ can be adjusted based on first-order information. This scheme is the essence of the shooting procedure.

Remark 1 *Let* $[\boldsymbol{x}(t), \boldsymbol{\lambda}(t)]^\top = \boldsymbol{\varphi}([\boldsymbol{x}_i, \boldsymbol{\lambda}_i]^\top, t_i, t)$ *be the solution of* (15) *integrated from* $[\boldsymbol{x}_i, \boldsymbol{\lambda}_i]^\top$, *initial time* t_i *to a generic time* t. *The optimization problem is stated as follows.*

$$\text{Find } \boldsymbol{\lambda}_i \text{ such that } [\boldsymbol{x}(t_f), \boldsymbol{\lambda}(t_f)]^\top = \boldsymbol{\varphi}([\boldsymbol{x}_i, \boldsymbol{\lambda}_i]^\top, t_i, t_f) \text{ satisfies }
\begin{cases}
\boldsymbol{r}(t_f) - \boldsymbol{r}_f = 0 \\
\boldsymbol{v}(t_f) - \boldsymbol{v}_f = 0 \\
\lambda_m(t_f) = 0.
\end{cases}
\tag{16}$$

6

More synthetically, the problem is to find $\boldsymbol{\lambda}_i$ such that $\boldsymbol{Z}(\boldsymbol{\lambda}_i) = 0$, where $\boldsymbol{Z}(\boldsymbol{\lambda})$, or the *shooting function*, is the seven-dimensional vector valued function given by the final boundary conditions (16). As finding the zeros of $\boldsymbol{Z}(\boldsymbol{\lambda})$ is not trivial, a number of techniques have to be implemented.

C.   Miniumu-Time Problem

A minimum-time step has to be solved to infer the minimum possible transfer time, $t_{f_{\min}}$, for each $T_{\max}$; see [10]. The minimum-fuel problem (16) has to be solved then for $t_f \geq t_{f_{\min}}$. The performance index of minimum-time problems is $J_t = \int_{t_i}^{t_f} 1 \, \mathrm{d}t$, and therefore the Hamiltonian reads

$$H_t = \boldsymbol{\lambda}_r \cdot \boldsymbol{v} + \boldsymbol{\lambda}_v \cdot \left[\boldsymbol{g}(\boldsymbol{r}) + \boldsymbol{h}(\boldsymbol{v}) + \frac{u\,T_{\max}}{m}\boldsymbol{\alpha} \right] - \lambda_m \frac{u\,T_{\max}}{c} + 1. \tag{17}$$

Applying the PMP to (17) yields

$$\begin{aligned} u^* &= 0 && \text{if } S_t > 0 \\ u^* &\in [0,1] && \text{if } S_t = 0 \\ u^* &= 1 && \text{if } S_t < 0, \end{aligned} \tag{18}$$

where the minimum-time switching function is

$$S_t = -\lambda_v \frac{c}{m} - \lambda_m. \tag{19}$$

When the final time is free, the transversality condition sets $H_t(t_f)$ to zero [25].

Remark 2 *The minimum-time problem is stated as follows.*

$$\text{Find } (\boldsymbol{\lambda}_i, t_f) \text{ such that } [\boldsymbol{x}(t_f), \boldsymbol{\lambda}(t_f)]^\top = \boldsymbol{\varphi}([\boldsymbol{x}_i, \boldsymbol{\lambda}_i]^\top, t_i, t_f) \text{ satisfies } \begin{cases} \boldsymbol{r}(t_f) - \boldsymbol{r}_f = 0 \\[4pt] \boldsymbol{v}(t_f) - \boldsymbol{v}_f = 0 \\[4pt] \lambda_m(t_f) = 0 \\[4pt] H_t(t_f) = 0. \end{cases} \tag{20}$$

III.   Analytic Derivatives

To increase accuracy and robustness of the shooting procedure, analytic derivatives are provided. In particular, the state transition matrix (STM) of (15), $\boldsymbol{\Phi}(t_i, t) = \mathrm{d}\boldsymbol{\varphi}(\boldsymbol{y}, t_i, t)/\mathrm{d}\boldsymbol{y}$, is derived. The STM maps small variations in the initial condition, $\delta\boldsymbol{y}_i$, over $t_i \to t$, i.e., $\delta\boldsymbol{y}(t) = \boldsymbol{\Phi}(t_i, t)\delta\boldsymbol{y}(t_i)$.

The STM is subject to the variational equation

$$\dot{\boldsymbol{\Phi}}(t_i, t) = D_{\boldsymbol{y}}\boldsymbol{F}\,\boldsymbol{\Phi}(t_i, t), \quad \boldsymbol{\Phi}(t_i, t_i) = \boldsymbol{I}_{14\times14}, \tag{21}$$

where $D_{\boldsymbol{y}}\boldsymbol{F}$, the Jacobian of $\boldsymbol{F}(\boldsymbol{y})$ in (15), has two different expressions: A) for $u^* = 0$ or $u^* = 1$ and B) for $u^* = (\varepsilon - S)/2$ (see Eqs. (12), (14), and (15)), i.e.

$$D_{\boldsymbol{y}}\boldsymbol{F}^{(A)} = \left[\begin{array}{cccc:ccc}
\boldsymbol{0} & \boldsymbol{I} & \boldsymbol{0} & \boldsymbol{0} & \boldsymbol{0} & \boldsymbol{0} \\
\boldsymbol{G} & \boldsymbol{H} & \frac{\boldsymbol{\lambda}_v}{\lambda_v}\frac{uT_{\max}}{m^2} & \boldsymbol{0} & -\frac{uT_{\max}}{m}\left(\frac{\boldsymbol{I}}{\lambda_v} - \frac{\boldsymbol{\lambda}_v\boldsymbol{\lambda}_v^\top}{\lambda_v^3}\right) & \boldsymbol{0} \\
\boldsymbol{0} & \boldsymbol{0} & 0 & \boldsymbol{0} & \boldsymbol{0} & 0 \\ \hdashline
-\frac{\partial(\boldsymbol{G}^\top\boldsymbol{\lambda}_v)}{\partial\boldsymbol{r}} & \boldsymbol{0} & \boldsymbol{0} & \boldsymbol{0} & -\boldsymbol{G}^\top & \boldsymbol{0} \\
\boldsymbol{0} & \boldsymbol{0} & \boldsymbol{0} & -\boldsymbol{I} & -\boldsymbol{H}^\top & \boldsymbol{0} \\
\boldsymbol{0} & \boldsymbol{0} & \frac{2\lambda_v uT_{\max}}{m^3} & \boldsymbol{0} & -\frac{\boldsymbol{\lambda}_v^\top}{\lambda_v}\frac{uT_{\max}}{m^2} & 0
\end{array}\right] \tag{22}$$

$$D_{\boldsymbol{y}}\boldsymbol{F}^{(B)} = \left[\begin{array}{cccc:ccc}
\boldsymbol{0} & \boldsymbol{I} & \boldsymbol{0} & \boldsymbol{0} & \boldsymbol{0} & \boldsymbol{0} \\
\boldsymbol{G} & \boldsymbol{H} & \boldsymbol{\Omega}_1 & \boldsymbol{0} & \boldsymbol{\Omega}_2 & \boldsymbol{\Omega}_3 \\
\boldsymbol{0} & \boldsymbol{0} & \boldsymbol{\Omega}_4 & \boldsymbol{0} & \boldsymbol{\Omega}_5 & \boldsymbol{\Omega}_6 \\ \hdashline
-\frac{\partial(\boldsymbol{G}^\top\boldsymbol{\lambda}_v)}{\partial\boldsymbol{r}} & \boldsymbol{0} & \boldsymbol{0} & \boldsymbol{0} & -\boldsymbol{G}^\top & \boldsymbol{0} \\
\boldsymbol{0} & \boldsymbol{0} & \boldsymbol{0} & -\boldsymbol{I} & -\boldsymbol{H}^\top & \boldsymbol{0} \\
\boldsymbol{0} & \boldsymbol{0} & \boldsymbol{\Omega}_7 & \boldsymbol{0} & \boldsymbol{\Omega}_8 & \boldsymbol{\Omega}_9
\end{array}\right] \tag{23}$$

where

$$\boldsymbol{\Omega}_1 = \frac{\boldsymbol{\lambda}_v}{\lambda_v}\frac{uT_{\max}}{m^2} + \frac{\boldsymbol{\lambda}_v cT_{\max}}{2\varepsilon m^3} \quad \boldsymbol{\Omega}_2 = -\frac{\boldsymbol{\lambda}_v\boldsymbol{\lambda}_v^\top}{\lambda_v^2}\frac{cT_{\max}}{2\varepsilon m^2} - \frac{uT_{\max}}{m}\left(\frac{\boldsymbol{I}}{\lambda_v} - \frac{\boldsymbol{\lambda}_v\boldsymbol{\lambda}_v^\top}{\lambda_v^3}\right) \quad \boldsymbol{\Omega}_3 = -\frac{\boldsymbol{\lambda}_v}{\lambda_v}\frac{T_{\max}}{2\varepsilon m}$$

$$\Omega_4 = \frac{\lambda_v T_{\max}}{2\varepsilon m^2} \qquad\qquad \boldsymbol{\Omega}_5 = -\frac{\boldsymbol{\lambda}_v^\top}{\lambda_v}\frac{T_{\max}}{2\varepsilon m} \qquad\qquad\qquad \Omega_6 = -\frac{T_{\max}}{2\varepsilon c}$$

$$\Omega_7 = \frac{2\lambda_v uT_{\max}}{m^3} + \frac{\lambda_v^2 cT_{\max}}{2\varepsilon m^4} \quad \boldsymbol{\Omega}_8 = -\frac{\boldsymbol{\lambda}_v^\top}{\lambda_v}\frac{uT_{\max}}{m^2} - \frac{\boldsymbol{\lambda}_v^\top cT_{\max}}{2\varepsilon m^3} \qquad\qquad \Omega_9 = -\frac{\lambda_v T_{\max}}{2\varepsilon m^2}.$$

Note that Eq. (21) is equivalent to 196 first-order differential equations for the elements of $\boldsymbol{\Phi}(t_i, t)$; it requires $D_{\boldsymbol{y}}\boldsymbol{F}$ to be evaluated along $\boldsymbol{y}(t)$, and therefore Eqs. (15) and (21) have to be integrated simultaneously. Let $\boldsymbol{z}$ be a vector containing $\boldsymbol{y}$ and columns of $\boldsymbol{\Phi}$; its first-order variation is

$$\dot{\boldsymbol{z}} = \mathcal{F}(\boldsymbol{z}) \quad \Rightarrow \quad \begin{bmatrix} \dot{\boldsymbol{y}} \\ \mathrm{vec}(\dot{\boldsymbol{\Phi}}) \end{bmatrix} = \begin{bmatrix} \boldsymbol{F}(\boldsymbol{y}) \\ \mathrm{vec}(D_{\boldsymbol{y}}\boldsymbol{F}\,\boldsymbol{\Phi}) \end{bmatrix}, \tag{24}$$

where 'vec' is an operator which converts the matrix into a column vector. Eqs. (24) yields 210 nonlinear differential equations. It is worth mentioning that $\boldsymbol{\Phi}(t_i, t)$ only maps states along a continuous orbit. If at time t_j there is a 'bang-bang' switching point, a discontinuity arises, and the STM across such discontinuity, $\boldsymbol{\Psi}(t_j)$, has to be determined. This STM can be computed as [9]

$$\boldsymbol{\Psi}(t_j) = \frac{\partial\boldsymbol{y}(t_j^+)}{\partial\boldsymbol{y}(t_j^-)} = \boldsymbol{I}_{14\times14} + \left(\dot{\boldsymbol{y}}|_{t_j^+} - \dot{\boldsymbol{y}}|_{t_j^-}\right)\left(\frac{\partial S}{\partial\boldsymbol{y}}\frac{1}{\dot{S}}\right)\bigg|_{t_j^-}, \tag{25}$$

where t_j^-, t_j^+ represent the times immediately before, after the discontinuity. In the likely case in which there are N 'bang-bang' points at times $t_1, \ldots, t_N$, the composite STM is given by [9]

$$\boldsymbol{\Phi}(t_f, t_i) = \boldsymbol{\Phi}(t_f, t_N^+)\boldsymbol{\Psi}(t_N)\boldsymbol{\Phi}(t_N^-, t_{N-1}^+)\boldsymbol{\Psi}(t_{N-1}) \ldots \boldsymbol{\Phi}(t_2^-, t_1^+)\boldsymbol{\Psi}(t_1)\boldsymbol{\Phi}(t_1^-, t_i) = \frac{\partial \boldsymbol{y}(t_f)}{\partial \boldsymbol{y}(t_i)}. \qquad (26)$$

IV.   Switching Detection Techniques

It has been mentioned that the right-hand side of Eq. (15) is discontinuous. When numerical integration is performed, discontinuities cause the integration error to accumulate about the switching points if these are not explicitly determined, which in turn threatens the entire shooting process. A hybrid switching detection technique combined with a variable step integration has been implemented to precisely detect the switching times. Let t_k, t_{k+1} be two consecutive integration steps and let $\boldsymbol{y}_k = \boldsymbol{y}(t_k)$, $\boldsymbol{y}_{k+1} = \boldsymbol{y}(t_{k+1})$. These states are linked through $\boldsymbol{y}_{k+1} = \boldsymbol{\varphi}_{\mathrm{RK}}(\boldsymbol{y}_k, t_k, t_{k+1})$, where $\boldsymbol{\varphi}_{\mathrm{RK}}$ is the numerical integration map. Let also t_{sw} be the switching time, and $S_k = S(\boldsymbol{y}(t_k))$, $S_{k+1} = S(\boldsymbol{y}(t_{k+1}))$ as per the switching function (12). With reference to Eq. (14), suppose that $S_k > \varepsilon$ and $-\varepsilon < S_{k+1} < \varepsilon$; extending the analysis to the other cases in Eq. (14) is straightforward. The focus is to determine the switching time t_{sw}, $t_{\mathrm{sw}} \in (t_k, t_{k+1})$, which zeroes $f(t_{\mathrm{sw}}) = S(t_{\mathrm{sw}}) - \varepsilon$.

The hybrid switching detection procedure developed is made of two steps. First, the Newton method is implemented because of its high efficiency; in general, only 4–5 iterations are needed to reach machine precision (i.e., 10^{-15}). The first guess is set to t_k and the analytic derivative in (13) is used. In case the Newton method fails or converges to solutions outside of the searching interval (t_k, t_{k+1}), a bisection procedure is executed. The latter is slower but more robust.

Algorithm 1 *The switching time, t_{sw}, is determined with the following procedure (Newton method).*

  i) Initialize $t_{\mathrm{sw}} = t_k$

  ii) Compute $t_{\mathrm{sw}} = t_{\mathrm{sw}} - f(t_{\mathrm{sw}})/\dot{S}(t_{\mathrm{sw}})$

  iii) Perform $\boldsymbol{y}(t_{\mathrm{sw}}) = \boldsymbol{\varphi}_{\mathrm{RK}}(\boldsymbol{y}_k, t_k, t_{\mathrm{sw}})$

  iv) Evaluate $f(t_{\mathrm{sw}})$ and $\dot{S}(t_{\mathrm{sw}})$ with $\boldsymbol{y}(t_{\mathrm{sw}})$

  v) Repeat steps ii)–iv) until $f(t_{\mathrm{sw}}) < \mathrm{tol}$
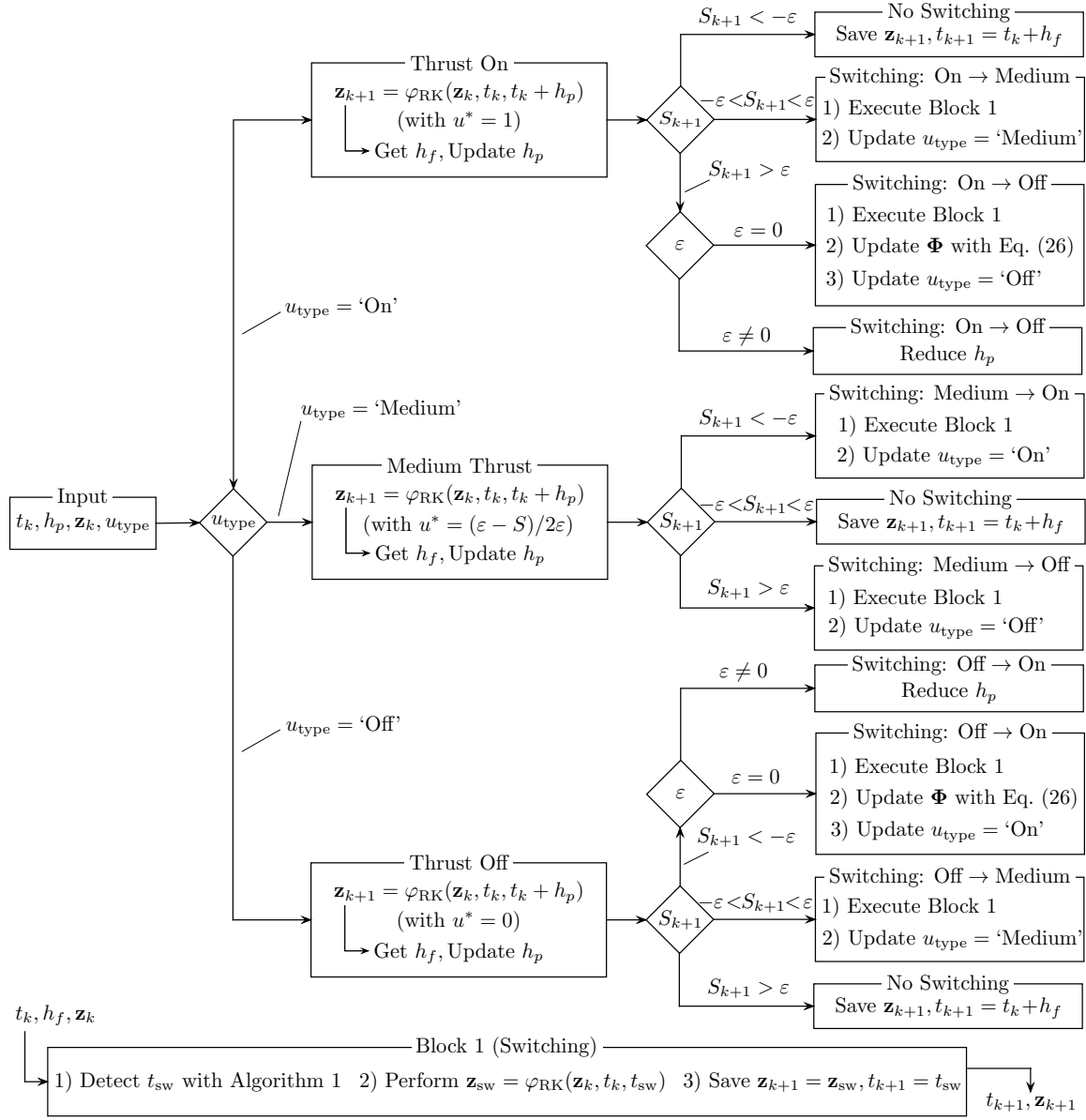
Fig. 1 Flow chart for the implementation of a generic integration step.

In case $f(t_{\mathrm{sw}}) > \mathrm{tol}$ or $t_{\mathrm{sw}} < t_k$ or $t_{\mathrm{sw}} > t_{k+1}$ execute a Bisection method within (t_k, t_{k+1}).

A. Practical Implementation

The low-thrust trajectory optimization problem has been implemented in a numerical framework. The 7th/8th-order Runge–Kutta scheme, with relative and absolute tolerances set to 10^{-14}, has been used to integrate Eqs. (15) and (21) (or equivalently Eqs. (24)), with the implicit optimal thrusting strategy in (14). The implementation of a generic integration step is outlined in Fig. 1.

The input required to execute an integration step are: 1) t_k, the initial integration time, 2) h_p, the step-size predicted at previous integration step (a value is guessed at first step), 3) $\boldsymbol{z}_k$, the 210-dimensional composite state at t_k (state and costate, $\boldsymbol{y}_k$, and the elements of $\boldsymbol{\Phi}(t_i, t_k)$, see Eqs. (24), 4) u_{type}, the logical thrust type at previous integration step, i.e., 'On', 'Medium', or 'Off' according to (14) (only 'On' or 'Off' in minimum-fuel problems). According to u_{type}, the flow is redirected to one of the three integration blocks in Fig. 1 where a prediction on $\boldsymbol{z}_{k+1}$ is made, $\boldsymbol{z}_{k+1} = \boldsymbol{\varphi}_{\text{RK}}(\boldsymbol{z}_k, t_k, t_k + h_p)$. Note that $\boldsymbol{z}_{k+1}$ is the composite state at time $t_{k+1} = t_k + h_f$, where h_f is the step-size corrected during the Runge–Kutta integration, which also updates the value of h_p for the subsequent integration. A correction is then made according to the value of the switching function S_{k+1}. The branch tagged with 'Thrust On' is analyzed for brevity. According to the relations (14), if $S_{k+1} < -\varepsilon$ the thrusting strategy is not changed over $[t_k, t_{k+1}]$, and therefore t_{k+1}, $\boldsymbol{z}_{k+1}$ are saved. When $-\varepsilon < S_{k+1} < \varepsilon$ a switching (from 'On' to 'Medium') occurs in $[t_k, t_{k+1}]$. In this case, the switching time, t_{sw}, as well as the state at the switching point, $\boldsymbol{z}_{\text{sw}}$, are detected with Algorithm 1, and u_{type} is updated (see 'Block 1' at the bottom of Fig. 1). In the case $S_{k+1} > \varepsilon$ two options are possible: a) in the minimum-energy problem ($\varepsilon \neq 0$) jumping from thrust 'On' to 'Off' is not possible, and therefore the step size has to be reduced and the process must be repeated; b) in the minimum-fuel problem ($\varepsilon = 0$) the switching time is detected, along with the state at the switching point, and the control type is updated. In the latter case, the STM is updated by considering the control discontinuity as in (25).

V.   Simulations and Results

The case study is a low-thrust transfer from a GTO to a L_1 halo orbit in the Earth–Moon system. The GTO has periapsis and apoapsis altitudes of $h_p = 400$ km and $h_a = 35,864$ km, respectively. The specific impulse is 3000 s, and the initial satellite mass is 1500 kg. The transfer begins at periapsis. From this point on, the low-thrust propulsion is used to increase the energy until a particular point on the halo orbit is targeted. Numerical experiments show that varying the target point has negligible impact over the total cost of the transfer. This orbit has an out-of-plane amplitude of 8000 km, and is consistent with [16–18, 20]. Table 1 summarizes the parameters used

in this work. The basis for distance, time, velocity, and mass units are the Earth–Moon distance, the inverse of their orbital angular velocity, the lunar circular speed, and the initial spacecraft mass, respectively. Table 2 reports the initial and final conditions.

Table 1 Physical constants.

Physical constant	Value
Mass parameter, μ	$1.21506683 \times 10^{-2}$
Gravitational field, g_0	9.80665 m/s^2
Length unit, LU	3.84405000×10^5 km
Time unit, TU	3.75676967×10^5 s
Speed unit, VU	1.02323281 km/s
Mass unit, MU	1500 kg

Table 2 Boundary conditions.

Boundary condition	Values
Initial position vector	$\boldsymbol{r}_i = [-0.019488511458668, -0.016033479812051, 0]^\top$ LU
Initial velocity vector	$\boldsymbol{v}_i = [8.918881923678198, -4.081793688818725, 0]^\top$ VU
Final position vector	$\boldsymbol{r}_f = [0.823385182067467, 0, -0.022277556273235]^\top$ LU
Final velocity vector	$\boldsymbol{v}_f = [0, 0.134184170262437, 0]^\top$ VU

A.   Minimum-Time Solutions

A minimum-time step is necessary to infer the minimum time required to accomplish the transfer, $t_{f_{\min}}$, for a given maximum thrust, $T_{\max}$. Once $t_{f_{\min}}$ is known, the subsequent energy-to-fuel optimization is formulated with a fixed final time t_f satisfying $t_f \geq t_{f_{\min}}$ at each $T_{\max}$. A continuation on $T_{\max}$ is performed. That is, at iteration k problem (20) is solved for a given value of thrust, and the pair $(\boldsymbol{\lambda}_i^{[k]}, t_{f_{\min}}^{[k]})$ is used as first guess solution in iteration $k + 1$, with decreased $T_{\max}$ (see Section II C). Solutions with $T_{\max}$ ranging from 10 N down to 0.3 N have been achieved, with transfer times that increase accordingly from 7.8 days to 171.6 days. The results, in terms of $t_{f_{\min}}$, m_f are reported in Table 3 for different $T_{\max}$, and their trend versus the initial thrust-to-mass ratio, $T_{\max}/m_i$, is drawn in Fig. 2. The transfer trajectories corresponding to $T_{\max}$ of 10 N, 2 N, 1

Table 3 Minimum-time solutions computed.

$T_{\max}$ (N)	$T_{\max}/m_i$ (m/s^2)	$t_{f_{\min}}$ (days)	m_f	Δv (km/s)
10	6.6667×10^{-3}	7.8549	0.8462	4.8015
9	6.0000×10^{-3}	8.6861	0.8469	4.7777
8	5.3333×10^{-3}	9.6522	0.8488	4.7133
7	4.6667×10^{-3}	10.8133	0.8518	4.6119
6	4.0000×10^{-3}	12.6278	0.8516	4.6186
5	3.3333×10^{-3}	12.9634	0.8730	3.9050
4	2.6667×10^{-3}	16.0510	0.8742	3.8655
3	2.0000×10^{-3}	21.1363	0.8758	3.8130
2	1.3333×10^{-3}	29.1512	0.8858	3.4865
1	6.6667×10^{-4}	56.2458	0.8898	3.3570
0.9	6.0000×10^{-4}	59.8376	0.8945	3.2055
0.8	5.3333×10^{-4}	64.6165	0.8987	3.0708
0.7	4.6667×10^{-4}	80.2242	0.8900	3.3505
0.6	4.0000×10^{-4}	87.6674	0.8970	3.1253
0.5	3.3333×10^{-4}	112.0327	0.8903	3.3408
0.4	2.6667×10^{-4}	138.4519	0.8915	3.3021
0.3	2.0000×10^{-4}	171.6254	0.8991	3.0580

N, and 0.6 N are reported in Fig. 3 in the Earth-centered frame. The throttle factor and switching function trends are instead reported in Fig. 4. In these solutions the thrust is always on; i.e., S_t in (19) is always negative, which triggers the last condition (18).

B. Minimum-Fuel Solutions

Minimum-fuel solutions are computed with a two-step continuation: 1) the minimum-energy problem ($\varepsilon = 1$) is solved iteratively with decreasing $T_{\max}$; 2) once a low-level of thrust is reached, ε is decreased until the minimum-fuel problem ($\varepsilon = 0$) is reached. Fig. 5 reports the thrust profile and switching function for the 10 steps needed to switch from minimum-energy to minimum-fuel, $T_{\max} = 10$ N. In this example, the continuation law is $\varepsilon_j = (j^2 - 1)/(N^2 - 1)$, with $j = 10, 9, \ldots, 2, 1$ and $N = 10$. The ability of the process in smoothing the thrust profile gradually is evident. For
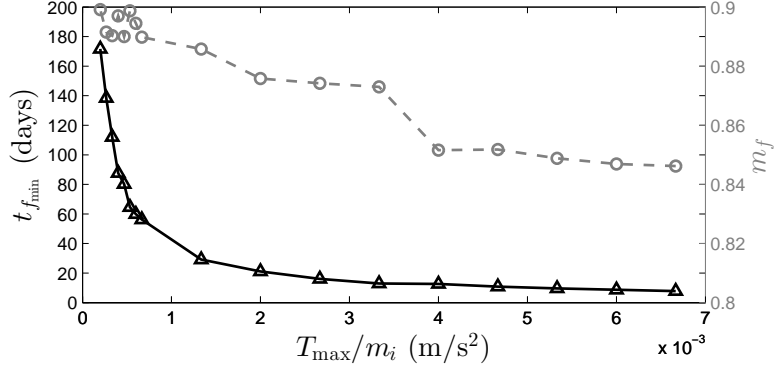
Fig. 2 Minimim transfer time, $t_{f_{\min}}$, and final mass ratio, m_f, versus thrust acceleration, $T_{\max}/m_i$, in minimum-time solutions.

each $T_{\max}$, the transfer time is chosen such that $t_f = c_{t_f} \times t_{f\min}$, where c_{t_f} is a coefficient selected manually. In step 2) above, varying c_{t_f} is a practical method to overcome convergence problems. The sensitivity of the final mass with respect to c_{t_f} is not considered.

For the sake of completeness, both minimum-energy and minimum-fuel solutions are reported for different values of $T_{\max}$ in Table 4. As expected, for each $T_{\max}$, minimum-fuel solutions use less propellant than minimum-energy ones. The solution with $T_{\max} = 0.6$ N has a thrust-to-mass ratio of $4 \times 10^{-4} \, \mathrm{m/s^2}$, which is consistent with the current state-of-the-art, and agrees with reference works [16–25]. This solution takes 140 days and needs just 8.5% of propellant mass fraction. Compared to the analogous minimum-time solution, this means saving 27 kg of propellant at the cost of spending additional 53 days of flight time.

Four sample minimum-fuel transfer trajectories are shown in Fig. 6 (rotating frame) and Fig. 7 (inertial frame). In both figures, the thick and thin lines indicate thrust and coast arcs, respectively. It can be seen that in the minimum-fuel solutions the thruster is on duty across the periapses (see Fig. 7). The algorithm is also capable of exploiting the stable structure associated to the halo orbit: all solutions foresee a final coast arc, which injects the spacecraft toward L_1 (the very final short thrust arc is the orbit injection maneuver, see Fig. 6). The long-duration, multi-spiral features of the low-thrust solutions can be appreciated in Figs. 6(d) and 7(d).

The trends for u and S corresponding to the solutions in Figs. 6 and 7 are reported in Fig. 8. The remarkable features of the low-thrust solution are proven in Figs. 6(d), 7(d) and 8(d): in
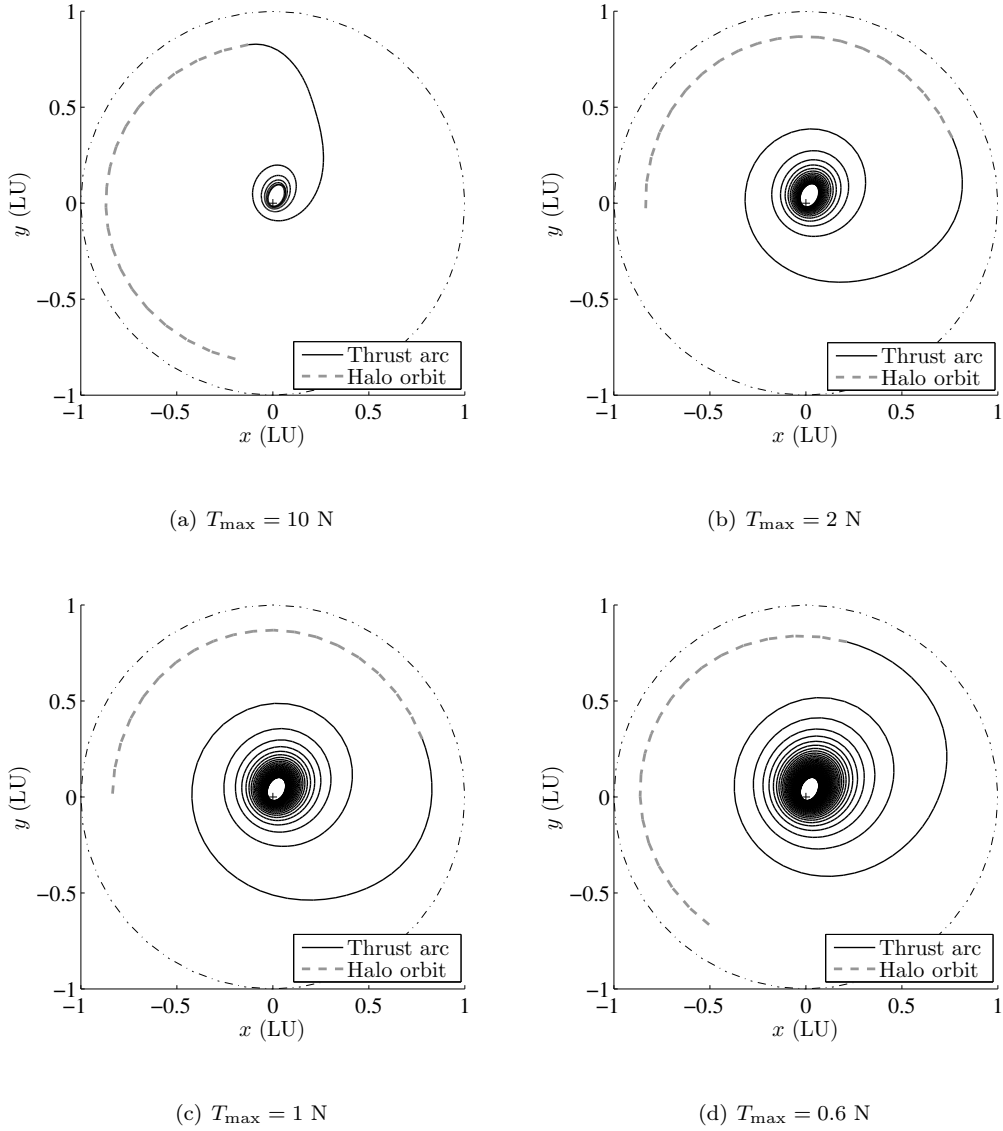
14

(a) $T_{\max} = 10$ N

(b) $T_{\max} = 2$ N

(c) $T_{\max} = 1$ N

(d) $T_{\max} = 0.6$ N

Fig. 3 Minimum-time trajectories for different values of $T\max$; Earth-centered inertial frame.

this solution the switching function S exhibits about 150 zero crossings, which cause 150 switching bang-bang structures in the throttle factor u, and about the same number of revolutions. The values of $\boldsymbol{\lambda}_i$ that allow solving Problem (16) are reported in Table 5 for all of the four cases presented.

VI. Conclusions

In this work, the formulation of low-thrust minimum-fuel, minimum-energy, and minimum-time trajectories in the restricted three-body problem is discussed, with applications to transfers from a geostationary transfer orbit to a halo orbit about L_1 in the Earth–Moon model. As these problems
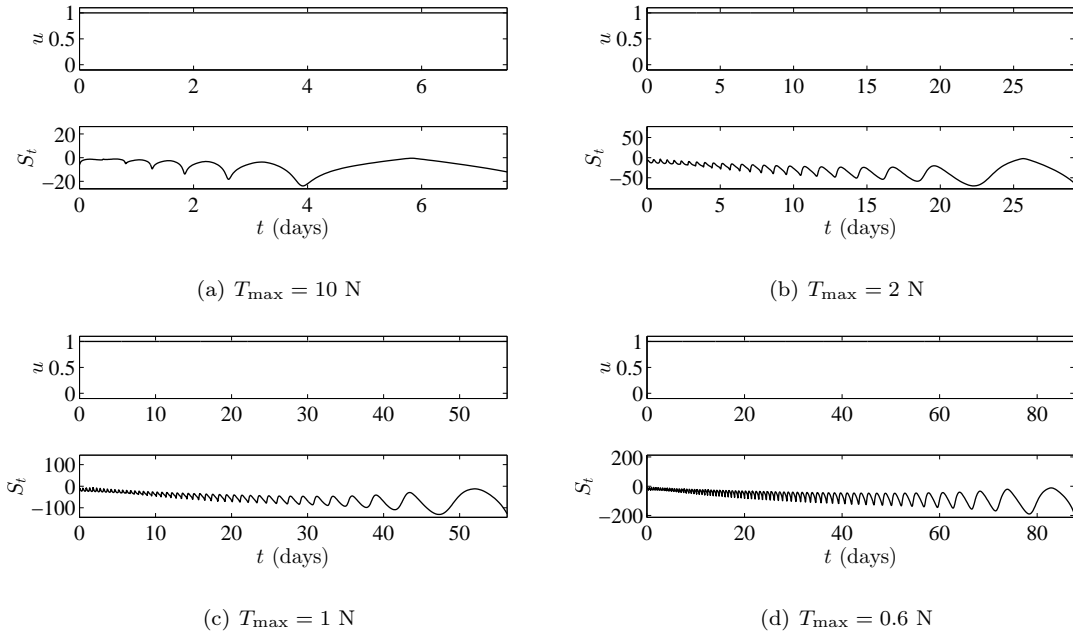
(a) $T_{\max} = 10$ N

(b) $T_{\max} = 2$ N

(c) $T_{\max} = 1$ N

(d) $T_{\max} = 0.6$ N

Fig. 4 Throttle factor, u, and switching function, S_t, profiles in minimum-time solutions.
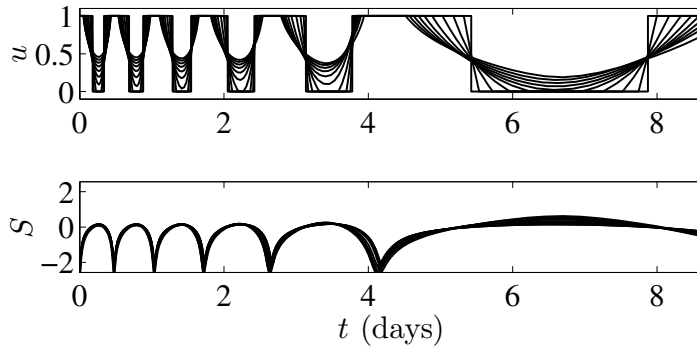

Fig. 5 Throttle factor, u, and switching function, S, for $T_{\max} = 10$ N.

pose several challenges, a number of issues allowing an effective and efficient implementation of a solution method are discussed. These techniques involve solving the minimum-time problem, introducing energy-to-fuel homotopy, formulating analytical derivatives, and implementing a hybrid method for accurate switching point detection.

A fixed point of the halo is targeted without exploiting its stable manifold. The algorithm is left free to place thrust arcs everywhere, and the existence of free coast arcs, mimicking the stable manifold, is found a posteriori. By the best of the authors' knowledge, these techniques have enabled solving, for the first time, the geostationary transfer orbit to halo low-thrust transfer *entirely*, so

16

Table 4 Solutions to minimum-energy ($\varepsilon = 1$) and minimum-fuel ($\varepsilon = 0$) cases, for different $T_{\max}$.

$T_{\max}$ (N)	$T_{\max}/m_i$ (m/s^2)	c_{t_f}	t_f (days)	m_f ($\varepsilon = 1$)	m_f ($\varepsilon = 0$)
10	6.6667×10^{-3}	1.1	8.6404	0.9034	0.9105
9	6.0000×10^{-3}	1.1	9.5548	0.9016	0.9103
8	5.3333×10^{-3}	1.1	10.6174	0.9003	0.9090
7	4.6667×10^{-3}	1.1	11.8946	0.8988	0.9072
6	4.0000×10^{-3}	1.2	15.1533	0.9009	0.9092
5	3.3333×10^{-3}	1.3	16.8524	0.8964	0.9053
4	2.6667×10^{-3}	1.3	20.8663	0.8936	0.9015
3	2.0000×10^{-3}	1.3	27.4773	0.8992	0.9088
2	1.3333×10^{-3}	1.3	37.8965	0.9091	0.9146
1	6.6667×10^{-4}	1.5	84.3688	0.9038	0.9131
0.6	4.0000×10^{-4}	1.6	140.2678	0.9069	0.9150

Table 5 Initial costate, $\boldsymbol{\lambda}_i$, and final time, t_f, for the four minimum-fuel solutions presented.

$T_{\max}$	$\boldsymbol{\lambda}_{r,i}$	$\boldsymbol{\lambda}_{v,i}$	$\lambda_{m,i}$	t_f (days)
10 N	$[15.616017, 32.875896, -0.094522]^\top$	$[-0.101606, 0.044791, -0.000150]^\top$	0.133266	8.6
2 N	$[6.476119, 13.589566, 0.133954]^\top$	$[-0.041598, 0.018240, -0.000162]^\top$	0.126720	37.8
1 N	$[4.229762, 10.873196, -0.420268]^\top$	$[-0.030411, 0.016232, 0.000094]^\top$	0.123321	84.3
0.6 N	$[3.728251, 9.861519, -0.412042]^\top$	$[-0.027239, 0.014900, -0.000007]^\top$	0.122115	140.2

avoiding splitting up the transfers into phases, which involves suboptimality.

References

[1] Mingotti, G., Topputo, F., and Bernelli-Zazzera, F., "Optimal Low-Thrust Invariant Manifold Trajectories via Attainable Sets," *Journal of Guidance, Control, and Dynamics*, Vol. 34, No. 6, 2011, pp.
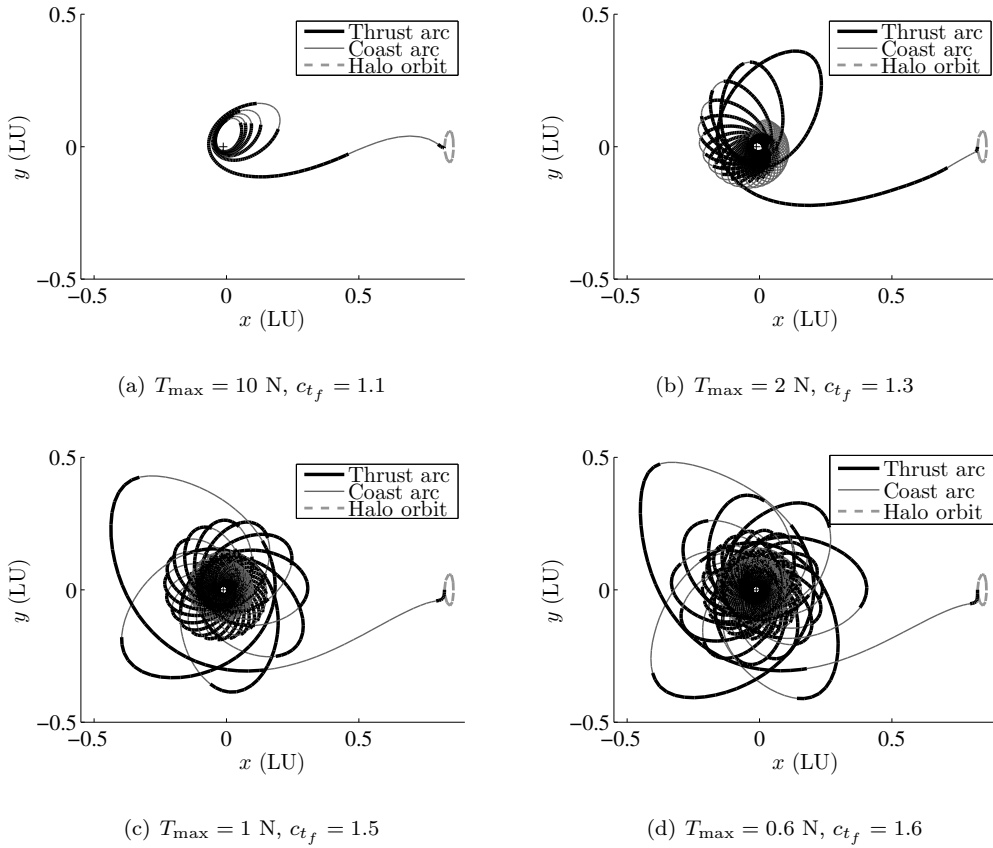
(a) $T_{\max} = 10$ N, $c_{t_f} = 1.1$

(b) $T_{\max} = 2$ N, $c_{t_f} = 1.3$

(c) $T_{\max} = 1$ N, $c_{t_f} = 1.5$

(d) $T_{\max} = 0.6$ N, $c_{t_f} = 1.6$

Fig. 6 Minimum-fuel trajectories for different values of $T_{\max}$; rotating frame.

1644–1656,

doi:10.2514/1.52493.

[2] Mingotti, G. and Gurfil, P., "Mixed Low-Thrust Invariant-Manifold Transfers to Distant Prograde Orbits around Mars," *Journal of Guidance, Control, and Dynamics*, Vol. 33, 2010, pp. 1753–1764, doi:10.2514/1.49810.

[3] Anderson, R. and Lo, M., "Role of Invariant Manifolds in Low-Thrust Trajectory Design," *Journal of Guidance, Control, and Dynamics*, Vol. 32, 2009, pp. 1921–1930, doi:DOI:10.2514/1.37516.

[4] Mingotti, G., Topputo, F., and Bernelli-Zazzera, F., "Low-Energy, Low-Thrust Transfers to the Moon," *Celestial Mechanics and Dynamical Astronomy*, Vol. 105, No. 1–3, 2009, pp. 61–74, doi:10.1007/s10569-009-9220-7.

[5] Mingotti, G., Topputo, F., and Bernelli-Zazzera, F., "Efficient Invariant-Manifold, Low-Thrust Planar Trajectories to the Moon," *Communication in Nonlinear Science and Numerical Simulation*, Vol. 17, No. 2, 2012, pp. 817–831,
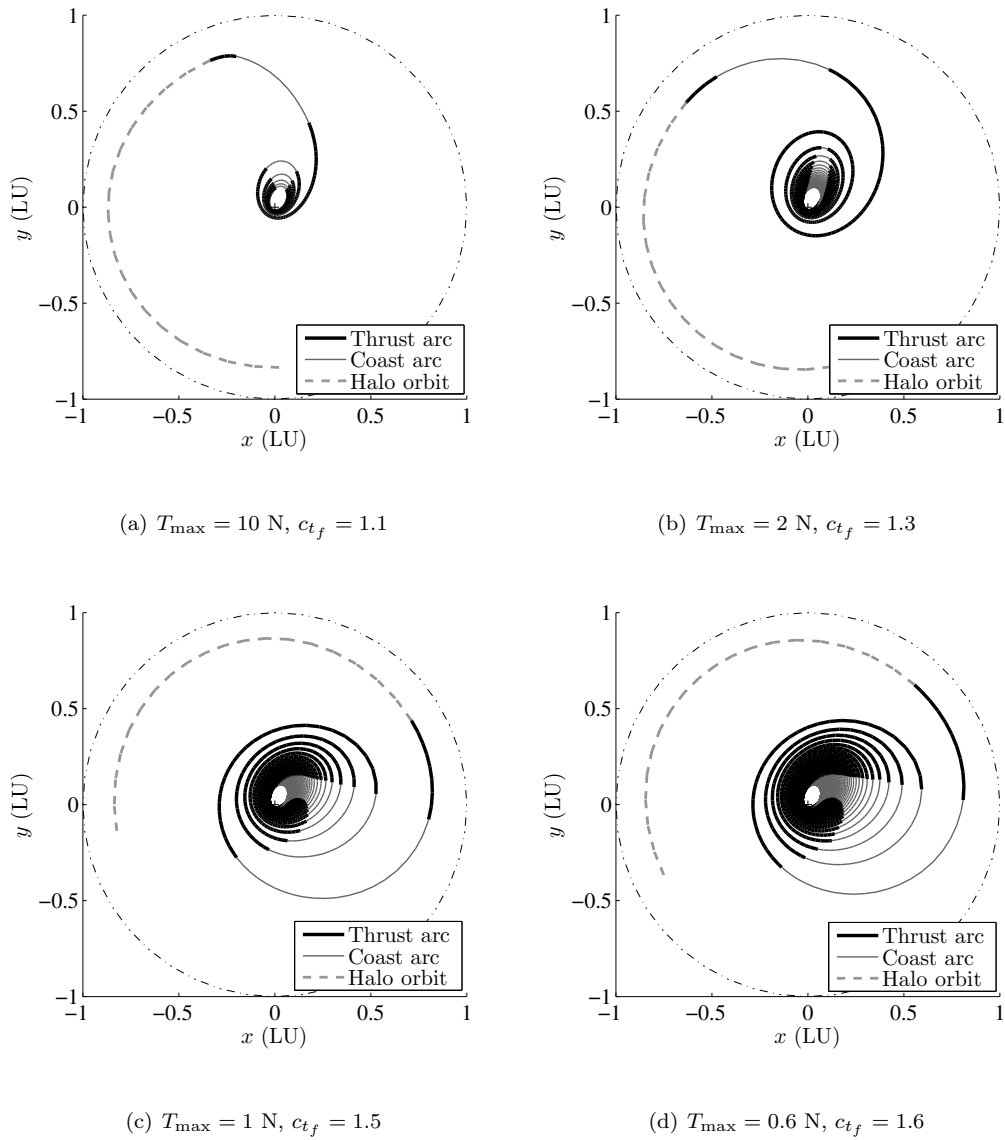
(a) $T_{\max} = 10$ N, $c_{t_f} = 1.1$ (b) $T_{\max} = 2$ N, $c_{t_f} = 1.3$

(c) $T_{\max} = 1$ N, $c_{t_f} = 1.5$ (d) $T_{\max} = 0.6$ N, $c_{t_f} = 1.6$

Fig. 7 Minimum-fuel **trajectories for different values of $T_{\max}$; Earth-centered inertial frame..**

doi:10.1016/j.cnsns.2011.06.033.

[6] Pierson, B. and Kluever, C., "Three-Stage Approach to Optimal Low-Thrust Earth–Moon Trajectories," *Journal of Guidance Control Dynamics*, Vol. 17, 1994, pp. 1275–1282, doi:10.2514/3.21344.

[7] Kluever, C. and Pierson, B., "Optimal Low-Thrust Three-Dimensional Earth–Moon Trajectories," *Journal of Guidance, Control, and Dynamcs*, Vol. 18, No. 4, 1995, pp. 830–837, doi:10.2514/3.21466.

[8] Herman, A. and Conway, B., "Optimal, Low-Thrust, Earth–Moon Orbit Transfer," *Journal of Guidance, Control, and Dynamics*, Vol. 21, No. 1, 1998, pp. 141–147,
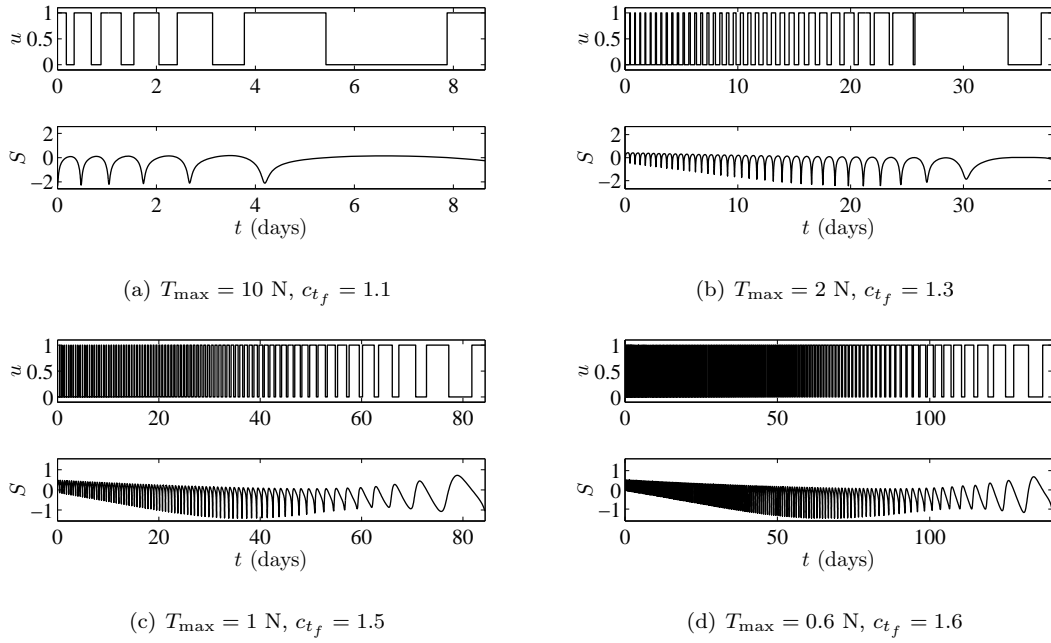
(a) $T_{\max} = 10$ N, $c_{t_f} = 1.1$

(b) $T_{\max} = 2$ N, $c_{t_f} = 1.3$

(c) $T_{\max} = 1$ N, $c_{t_f} = 1.5$

(d) $T_{\max} = 0.6$ N, $c_{t_f} = 1.6$

Fig. 8 **Throttle factor, u, and switching function, S, profiles in minimum-fuel solutions.**

doi:10.2514/2.4210.

[9] Russell, R., "Primer Vector Theory Applied to Global Low-Thrust Trade Studies," *Journal of Guidance, Control, and Dynamics*, Vol. 30, No. 2, 2007, pp. 460–472,

doi:10.2514/1.22984.

[10] Caillau, J., Daoud, B., and Gergaud, J., "Minimum Fuel Control of the Planar Circular Restricted Three-Body Problem," *Celestial Mechanics and Dynamical Astronomy*, Vol. 114, No. 1-2, 2012, pp. 137–150,

doi:10.1007/s10569-012-9443-x.

[11] Schoenmaekers, J., Horas, D., and Pulido, J., "SMART-1: With Solar Electric Propulsion to the Moon," in "Proceeding of the 16th International Symposium on Space Flight Dynamics," , 2001, pp. 1–14.

[12] Belbruno, E., "Lunar Capture Orbits, a Method of Constructing Earth–Moon Trajectories and the Lunar GAS Mission," in "Proceedings of the AIAA/DGLR/JSASS International Electric Propulsion Conference," , 1987, pp. 97–1054.

[13] Condon, G. and Pearson, D., "The Role of Humans in Libration Point Missions With Specific Application to an Earth-Moon Libration Point Gateway Station," *Advances in the Astronautical Sciences*, Vol. 109, No. 1, 2001, pp. 95–110.

[14] Farquhar, R., Dunham, D., Guo, Y., and McAdams, J., "Utilization of Libration Points for Human Exploration in the Sun–Earth–Moon System and Beyond," *Acta Astronautica*, Vol. 55, No. 3–9, 2004,

pp. 687–700,

doi:10.1016/j.actaastro.2004.05.021.

[15] Post, K., Belbruno, E., and Topputo, F., "Efficient Cis-Lunar Trajectories," in "Global Space Exploration Conference, Paper GLEX-2012.02.3.6x12248, Washington, DC, USA," , 2012, pp. 1–19.

[16] Mingotti, G., Topputo, F., and Bernelli-Zazzera, F., "Combined Optimal Low-Thrust and Stable-Manifold Trajectories to the Earth–Moon Halo Orbits," *AIP Conference Proceedings*, Vol. 886, 2007, pp. 100–110,

doi:10.1063/1.2710047.

[17] Armellin, R. and Topputo, F., "A Sixth-Order Accurate Scheme for Solving Two-Point Boundary Value Problems in Astrodynamics," *Celestial Mechanics and Dynamical Astronomy*, Vol. 96, No. 3–4, 2006, pp. 289–309,

doi:10.1007/s10569-006-9047-4.

[18] Martin, C. and Conway, B., *Spacecraft Trajectory Optimization*, Cambridge University Press, UK, chap. Optimal Low-Thrust Trajectories Using Stable Manifolds, pp. 238–262, 2010.

[19] Pergola, P., Finocchietti, C., and Andrenucci, M., "Design of Low-Thrust Transfers to Libration Point Periodic Orbits Exploiting Manifold Dynamics," *Advances in the Astronautical Sciences*, Vol. 145, 2012, pp. 421–436.

[20] Rasotto, M., Armellin, R., Di Lizia, P., and Bernelli-Zazzera, F., "Optimal Low-Thrust Transfers in Two-Body and Three-Body Dynamics," in "64th International Astronautical Congress," Curran Associates, Red Hook, NY, 2013, pp. 5230–5244.

[21] Starchville, T. and Melton, R., "Optimal Low-Thrust Trajectories to Earth-Moon L2 Halo Orbits (Circular Problem)," in "Proceedings of the AAS/AIAA Astrodynamics Specialists Conference," , 1997, pp. 97–714.

[22] Senent, J., Ocampo, C., and Capella, A., "Low-Thrust Variable-Specific-Impulse Transfers and Guidance to Unstable Periodic Orbits," *Journal of Guidance, Control, and Dynamics*, Vol. 28, 2005, pp. 280–290,

doi:10.2514/1.6398.

[23] Ozimek, M. and Howell, K., "Low-Thrust Transfers in the Earth–Moon System Including Applications to Libration Point Orbits," *Journal of Guidance, Control, and Dynamics*, Vol. 33, No. 2, 2010, pp. 533–549,

doi:10.2514/1.43179.

[24] Abraham, A., Spencer, D., and Hart, T., "Preliminary Optimization of Low-Thrust, Geocentric to

Halo Orbit, Transfers via Particle Swarm Optimization," in "24th AAS/AIAA Space Flight Mechanics Meeting, Santa Fe, New Mexico, 26–30 January," , 2014, pp. 1–17.

[25] Caillau, J. and Daoud, B., "Minimum Time Control of the Restricted Three-Body Problem," *SIAM Journal on Control and Optimization*, Vol. 50, No. 6, 2012, pp. 3178–3202, doi:10.1137/110847299.

[26] Bertrand, R. and Epenoy, R., "New Smoothing Techniques for Solving Bang–Bang Optimal Control Problemsâ Numerical Results and Statistical Interpretation," *Optimal Control Applications and Methods*, Vol. 23, No. 4, 2002, pp. 171–197, doi:10.1002/oca.709.

[27] Haberkorn, T., Martinon, P., and Gergaud, J., "Low Thrust Minimum-Fuel Orbital Transfer: a Homotopic Approach," *Journal of Guidance, Control, and Dynamics*, Vol. 27, No. 6, 2004, pp. 1046–1060, doi:10.2514/1.4022.

[28] Jiang, F., Baoyin, H., and Li, J., "Practical Techniques for Low-Thrust Trajectory Optimization with Homotopic Approach," *Journal of Guidance, Control, and Dynamics*, Vol. 35, No. 1, 2012, pp. 245–258, doi:10.2514/1.52476.

[29] Martinon, P. and Gergaud, J., "SHOOT2.0: An Indirect Grid Shooting Package for Optimal Control Problems, with Switching Handling and Embedded Continuation," Tech. Rep. 7380, Institut National de Recherche en Informatique et an Automatique, 2010.

[30] Mantia, L. and Casalino, L., "Indirect Optimization of Low-Thrust Capture Trajectories," *Journal of Guidance, Control, and Dynamcs*, Vol. 29, No. 4, 2006, pp. 1011–1014, doi:10.2514/1.18986.

[31] Casalino, L., Colasurdo, G., and Pastrone, D., "Optimal Low-Thrust Escape Trajectories Using Gravity Assist," *Journal of Guidance, Control, and Dynamics*, Vol. 22, No. 5, 1999, pp. 637–642, doi:10.2514/2.4451.

[32] Szebehely, V., *Theory of Orbits: The Restricted Problem of Three Bodies*, Academic Press Inc., 1967, pp. 7–29.

[33] Prussing, J., *Spacecraft Trajectory Optimization*, Cambridge University Press Cambridge, UK, chap. Primer Vector Theory and Applications, pp. 16–36, 2010.

[34] Thevenet, B. and Epenoy, R., "Minimum-Fuel Deployment for Spacecraft Formations via Optimal Control," *Journal of Guidance, Control, and Dynamics*, Vol. 31, No. 1, 2008, pp. 101–113, doi:10.2514/1.30364.

[35] Bryson, A. and Ho, Y., *Applied Optimal Control*, John Wiley & Sons, New York, 1975, pp. 42–89.

[36] Pontryagin, L., *Mathematical Theory of Optimal Processes*, Interscience Publishers, New York, 1962 pp. 1–114.

[37] Lawden, D., *Optimal Trajectories for Space Navigation*, Butterworths, London, 1963 pp. 1–59.